The Journal of Immunology

Distinct Binding Affinities of Mac-1 and LFA-1 in Neutrophil Activation

Ning Li, Debin Mao, Shouqin Lü, Chunfang Tong, Yan Zhang and Mian Long

J Immunol 2013; 190:4371-4381; Prepublished online 20 March 2013;
doi: 10.4049/jimmunol.1201374
http://www.jimmunol.org/content/190/8/4371

Supplementary Material http://www.jimmunol.org/content/suppl/2013/03/20/jimmunol.1201374.DC1

References This article **cites 51 articles**, 27 of which you can access for free at:
http://www.jimmunol.org/content/190/8/4371.full#ref-list-1

The Journal of Immunology is published twice each month by
The American Association of Immunologists, Inc.,
1451 Rockville Pike, Suite 650, Rockville, MD 20852

Print ISSN: 0022-1767 Online ISSN: 1550-6606.

Distinct Binding Affinities of Mac-1 and LFA-1 in Neutrophil Activation

Ning Li, Debin Mao, Shouqin Lü, Chunfang Tong, Yan Zhang, and Mian Long

Macrophage-1 Ag (Mac-1) and lymphocyte function-associated Ag-1 (LFA-1), two β_2 integrins expressed on neutrophils (PMNs), mediate PMN recruitment cascade by binding to intercellular adhesive molecule 1. Distinct functions of LFA-1–initiating PMN slow rolling and firm adhesion but Mac-1–mediating cell crawling are assumed to be governed by the differences in their binding affinities and kinetic rates. In this study, we applied an adhesion frequency approach to compare their kinetics in the quiescent and activated states using three molecular systems, constitutively expressed receptors on PMNs, wild-type and high-affinity (HA) full-length constructs transfected on 293T cells, and wild-type and HA recombinant extracellular constructs. Data indicate that the difference in binding affinity between Mac-1 and LFA-1 is on-rate dominated with slightly or moderately varied off-rate. This finding was further confirmed when both β_2 integrins were activated by chemokines (fMLF or IL-8), divalent cations (Mg^{2+} or Mn^{2+}), or disulfide bond lockage on an HA state. Structural analyses reveal that such the kinetics difference is likely attributed to the distinct conformations at the interface of Mac-1 or LFA-1 and intercellular adhesive molecule 1. This work furthers the understandings in the kinetic differences between Mac-1 and LFA-1 and in their biological correlations with molecular activation and structural bases. ***The Journal of Immunology*****, 2013, 190: 4371–4381.**

The β_2 integrin is crucial to many biological processes such as inflammatory cascade and tumor metastasis (1, 2). For example, macrophage-1 Ag (Mac-1, $\alpha_M\beta_2$, and CD11b/CD18) and lymphocyte function-associated Ag-1 (LFA-1, $\alpha_L\beta_2$, and CD11a/CD18) are found to regulate neutrophil (PMN) recruitment (3), lymphocyte homing (4), monocyte crawling (5), and tumor cell embedding (6). The two molecules share common β_2-subunit noncovalently associated with respective α subunit. β_2-Subunit is composed of an I-like domain, a hybrid domain, a plexin/semaphorin/integrin domain, four integrin-EGF domains, a transmembrane domain, and a cytoplasmic tail, whereas α-subunit includes an inserted domain (I domain), a β-propeller, a thigh domain, two calf domains, a transmembrane domain, and a cytoplasmic tail. Inserted domain (I domain) of α-subunit contains the binding pocket to their various ligands, including intercellular adhesive molecules (1, 2, 7). Intercellular adhesive molecule 1 (ICAM-1), a member of super-IgG family, consists of five IgG-like domains (D1–D5) and binds to Mac-1 via D3 domain (8) and LFA-1 via D1 domain (9), respectively.

Physiologically, Mac-1 and LFA-1 are constitutively expressed on PMNs and initiate the slow rolling, firm adhesion, and transient crawling of PMNs via binding to ICAM-1 ligands expressed on activated endothelial cells under blood flow (7, 10, 11). Even with similar structures, Mac-1 and LFA-1 play distinct roles in leukocyte activation. For example, LFA-1 mediates neutrophil slow rolling and firm adhesion, but Mac-1 governs following intraluminal crawling (12–15). LFA-1 also supports monocyte firm adhesion and crawling in quiescent condition, whereas Mac-1 is responsible for TNF-α–stimulated monocyte crawling (16). Multiple functional states of LFA-1 with different affinities are required for lymphocyte rolling, adhesion, and crawling because no Mac-1 molecules are presented onto lymphocyte surface (17–20). These observations bring up a question why the two structurally similar β_2 integrins behave distinctly in leukocyte recruitment and what the underlying mechanisms are.

Such the functional differences are more likely observed in leukocyte activation, which is associated with various functional states of β_2 integrins. Inside-out signaling triggered by selectins and chemokines or outside-in signaling triggered by ligand binding induces integrins to undergo dramatic transition from bent low-affinity (LA) to extended intermediate- or high-affinity (HA) conformation, which leads to opening of the ligand-binding pocket. Binding of activated integrins to their ligands on endothelial cells favors neutrophil arrest and firm adhesion (1, 2, 7, 10, 11). Furthermore, Mac-1 and LFA-1 are found to respond diversely to different chemokines: Mac-1 is the dominant integrin involved in chemotaxis to fMLF, whereas LFA-1 is the major receptor involved in chemotaxis to IL-8 (21). LFA-1 responds within first 300 s after IL-8 stimulation, whereas Mac-1 begins to be engaged in from 350 s after activation (22). Expression of Mac-1 (but not of LFA-1) is rapidly increased after chemotactic stimulation by presenting Mac-1 from secretory granules to cell surface (23). These findings suggest that both the activated β_2 integrins also present distinct features.

Although a body of evidences has been found to focus on the functional differences between Mac-1 and LFA-1 using in vivo, ex vivo, and in vitro measurements (12–23), it is still hard to provide a mechanistic insight. One way to elucidate the underlying mechanisms is to quantify the binding kinetics because it determines

Key Laboratory of Microgravity (National Microgravity Laboratory) and Center of Biomechanics and Bioengineering, Institute of Mechanics, Chinese Academy of Sciences, Beijing 100190, China

Received for publication May 16, 2012. Accepted for publication February 13, 2013.

This work was supported by National Natural Science Foundation of China Grant 31230027 and National Key Basic Research Foundation of China Grant 2011CB710904.

Address correspondence and reprint requests to Dr. Mian Long, Key Laboratory of Microgravity (National Microgravity Laboratory) and Center of Biomechanics and Bioengineering, Institute of Mechanics, Chinese Academy of Sciences, No. 15 North 4th Ring Road, Beijing 100190, China. E-mail address: mlong@imech.ac.cn

The online version of this article contains supplemental material.

Abbreviations used in this article: HA, high-affinity; ICAM-1, intercellular adhesive molecule 1; I domain, inserted domain; LA, low-affinity; LFA-1, lymphocyte function-associated Ag-1; Mac-1, macrophage-1 Ag; MD, molecular dynamic; MIDAS, metal ion-dependent adhesion site; PMN, neutrophil; WT, wild-type.

the on- and off-rates and binding affinity of interacting molecules. In this study, we hypothesize that the distinct roles of Mac-1 and LFA-1 are likely attributed to the differences in the binding kinetics to ICAM-1. We compared the ICAM-1 binding between Mac-1 and LFA-1 in three systems: constitutive β_2 integrins expressed on neutrophils, full-length receptors transfected on 293T cells, or recombinant soluble receptors immobilized on microbeads. Also investigated was their corresponding conformational dynamics that determines the binding kinetics. The outcomes provide a new insight in understanding the molecular mechanism for their distinct functions and structure–function relationship.

Materials and Methods

Reagents and cells

Recombinant human ICAM-1 with or without Fc was purchased from R&D Systems (Minneapolis, MN). Mouse anti-human CD11a mAb 27, anti-CD11b mAbs bear-1, 23F-12, anti-CD18 mAb L-13, used for ELISA and Western blot tests (compare Supplemental Fig. 3A, 3B), anti-CD11b blocking mAb ICRF44, anti–ICAM-1 blocking mAb 8.4A6, used for binding specificity tests (compare Supplemental Fig. 3D), and biotin-labeled goat–anti-human IgG polyclonal Ab were from Santa Cruz Biotechnology (Santa Cruz, CA). Anti-human CD11a blocking mAb MEM-25 and anti-human CD18 blocking mAb TS1/18 were from Enzo Life Sciences (Farmingdale, NY) and BioLegend (San Diego, CA), respectively. FITC-labeled mouse–anti-human ICAM-1 mAb BBIG-I1, mouse-anti-human CD18 mAb MEM-148, and goat–anti-mouse IgG polyclonal Ab were from R&D Systems (Minneapolis, MN), GeneTex (Irvine, CA), and Sigma-Aldrich (Seattle, WA), respectively. Goat–anti-human IgG Fc polyclonal Ab was from Abcam (Cambridge, U.K.). Peroxidase-conjugated secondary polyclonal Ab used for ELISA and Western blot tests was from Boster (Wuhan, China).

Human kidney epithelial 293T cells were purchased from the American Type Culture Collection (Manassas, VA). Human neutrophils were isolated from whole blood samples using a Ficoll–Hypaque density gradient (Histopaque-1077 and Histopaque-1119 from Sigma-Aldrich) as described previously (24). Collected PMNs were directly used for binding kinetics tests without further lysing RBCs to minimize the activation of PMNs. To isolate the impact of Mac-1 or LFA-1, the cells were preincubated respectively with anti–LFA-1 (clone MEM-25) or anti–Mac-1 (clone ICRF44) blocking mAbs for 1 h on ice and then suspended in HBSS with Ca^{2+} and Mg^{2+} containing 2% FBS. In the cases of PMN binding, Fab fragments of the blocking mAbs were generated from whole IgG by using the Fab preparation kit following the manufacturer's instructions (Thermo Fisher Scientific, Waltham, MA). In the tests of chemokines impact, the PMNs were pretreated with 10 nM fMLF or 10 nM IL-8 for 20 min prior to adding in blocking Abs. In the tests of metal ion effect, the PMNs were suspended in 1 mM Mg^{2+} or 1 mM Mn^{2+} in the presence of Ca^{2+}- and Mg^{2+}-free HBSS containing 2% FBS and 1 mM EGTA (Supplemental Fig. 1A).

Reconstruction and expression of full-length and extracellular β_2 integrins

Full-length cDNA constructs encoding human wild-type (WT) CD11b (in pEYFP-N1) and CD18 (in pECFP-N1) were gifts from Dr. C. He (Second Military Medical University, Shanghai, China). Human IgG1 Fc domain cDNA (in pcDNA3.1) was a gift from Dr. Y. Li (Academy of Military Medical Sciences, Beijing, China). The full-length CD11a cDNA was obtained by RT-PCR from human PMNs. The HA mutants (Q163C/Q309C point mutagenesis for Mac-1 and K287C/K294C for LFA-1) were constructed by substituting corresponding amino acids with cysteines in CD11b and CD11a, respectively, as described previously (25, 26). Four distinct α-subunits so constructed and one common β-subunit full-length plasmid including extracellular domains, transmembrane segment, and cytoplasmic tail were then reconstructed into pcDNA3.1, and named as WT Mac-1, HA Mac-1, WT LFA-1, and HA LFA-1, respectively (Supplemental Fig. 1B). The entities of four recombinant β_2 integrins were confirmed by gene sequencing (Sangon Biotech, Shanghai, China) (data not shown). Each pair of one α-subunit and one β-subunit plasmids was cotransfected into 293T cells via a calcium phosphate-mediated transfection procedure (Promega, Madison, MI), whereas mock plasmid without target gene was used as control. Briefly, 293T cells were seeded into 6-well plates 1 d before transfection and grew to 60∼80% confluence. A total of 6 μg of the corresponding α and β plasmids were cotransfected for each well. The cells were then cultured at 37˚C in a humidified atmosphere of 5% CO_2 (v/v) for 48 h. Harvested cells were segregated into two aliquots: one was used for binding kinetics tests to estimate kinetic parameters and the other was used for flow cytometry measurements to determine the integrin densities where the distinct mAb of MEM-25, ICRF44, or TS1/18 was used for staining CD11a, CD11b, or CD18, respectively.

To construct the chimera of Mac-1 or LFA-1 with Fc domain, three fragments encoding the ectodomains of CD11a (Gln-1063), CD11b (Leu-1093), and CD18 (Asn-678) were, respectively, cloned into pcDNA3.1 vectors (Supplemental Fig. 1C), in which the Fc domain containing T366Y or Y407T mutation was fused to C-terminal of α- or β-subunit for reserving the likelihood of heterodimerization between α- and β- chains (27). The entities of four recombinant Fc chimeras so constructed, namely WT Mac-1-Fc, WT LFA-1-Fc, HA Mac-1-Fc (Q163C/Q309C), and HA LFA-1-Fc (K287C/K294C), were also confirmed (data not shown). Then the plasmids were respectively transfected into 293T cells and culture supernatant was collected after 96 h culture by centrifugation at $1000 \times g$. The soluble β_2 integrin–Fc chimeras were harvested via anti-Fc secondary Ab precoated on microbeads.

In some cases, S144E mutation in Mac-1-Fc and S141F mutation in LFA-1-Fc were generated by QuikChange Lightning site-directed mutagenesis kit (Agilent, Santa Clara, CA) and verified by DNA sequencing (data not shown).

Site density determination

Site densities of Mac-1 and LFA-1 expressed on PMNs or 293T cells or coated on microbeads were determined by flow cytometry. Three aliquots of PMNs or 293T cells or microbeads were respectively incubated with anti-CD11a (clone MEM-25), anti-CD11b (clone ICRF44), and anti-CD18 (clone TS1/18) mAbs at a concentration of 10 μg/ml for 1 h on ice. The cells or microbeads were then incubated with FITC-conjugated goat–anti-mouse secondary Ab for 30 min on ice. Washed cells or microbeads were analyzed by flow cytometer (Becton Dickinson Biosciences, San Jose, CA). For ICAM-1s, the dimeric ICAM-1-Fc was captured via pre-absorbed goat–anti-human IgG Fc polyclonal Ab on 3-μm-diameter glass microbeads, whereas monomeric ligands were physically absorbed on 6-μm-diameter polystyrene microbeads (Supplemental Fig. 1D). The microbeads were then incubated with FITC-labeled mouse–anti-human ICAM-1 mAb (BBIG-I1) and also analyzed by flow cytometer. Analysis was done by gating on the cell or microbead population, and the fluorescent intensities of the cells or microbeads were then used to determine their site densities, where the calibration curve was obtained by running standard beads (Bangs, Fishers, IN) (Supplemental Fig. 2D). Site density of β_2 integrins or ICAM-1s were calculated using m_r or $m_l = (S \times GMFI)/[4\pi r^2 \times (F/P)]$, where S denotes the slope of calibration curve, $GMFI$ is the geometric mean fluorescence intensity, r is the cell or microbead radius, and F/P is the equivalent of fluorochromes per protein.

Binding kinetics measurements

An adhesion frequency assay, used to determine the kinetic rates and binding affinity of surface-bound molecule pair, has been described previously (24, 28, 29). Briefly, each 10^3 PMNs (or 293T cells) and ICAM-1–coupled microbeads were mixed just before injecting into a customer-made sample chamber (∼$14 \times 10 \times 0.5$ cm). A floating 3-μm glass microbead coupled by ICAM-1-Fc via anti-Fc Ab was captured by a mobile optical trap (Carl Zeiss, Munich, Germany). A cell settled down to adhere stably onto the coverslip substrate and was then brought by a computer-controlled piezoelectric actuator (Physik Instrumente, Karlsruhe, Germany) into contact repeatedly with ICAM-1–bearing microbead. In some cases, a 6-μm polystyrene microbead physically adsorbing ICAM-1 was immobilized onto the substrate and a 3-μm streptavidin-coated polystyrene microbead, which preabsorbed biotin-labeled goat–anti-human IgG polyclonal Ab and then captured Fc-fused recombinant β_2 integrins, was captured by the trap. The measurements were done at room temperature ranging 25–30˚C. The interactions between ICAM-1 and β_2 integrins were measured at a given contact duration for one cell–microbead or microbead–microbead pair but varied over a range (0.25∼7.0 s) for different pairs. The presence of adhesion at the end of a given contact period was detected mechanically by observing microscopically the rebounding of the microbead back to the trap center upon retracting it. This contact–retraction cycle was repeated 50∼100 times to estimate the adhesion probability, P_a, at that contact duration, t. For each case examined, totally 21∼90 pairs were applied to obtain one or two P_a versus t curves that correspond to varied integrin densities, m_r, and ICAM-1 density, m_l. Each binding curve was fitted to a small system probabilistic kinetic model (29),

$$P_a = 1 - \exp\{-m_r m_l A_c K_a [1 - \exp(-k_r t)]\}, \quad (1)$$

to estimate a pair of parameters: the off-rate, k_r and the binding affinity, A_cK_a. In this study, A_c is the contact area between one and another cell or bead, which was kept constant in all experiments, and m_r and m_l are site densities per unit area of β_2 integrin receptors and ICAM-1 ligands, respectively. The on-rate was obtained by calculating from $A_ck_f = A_cK_a \times k_r$. The best fit of measured data to Eq. 1 and the 95% confidence intervals of the best-fit curves were performed by Sigma-Plot (Systat Software, San Jose, CA), and the estimated parameters are presented as the mean ± SEM. The binding affinity A_cK_a reported in this study is denoted as the effective affinity mediated by per β_2 integrin and ICAM-1 pair, which is independent of molecular densities of interacting receptors and ligands. In some cases, two pairs of (A_cK_a, k_r) values were obtained at two different site densities to allow evaluation of the mean and SEM of kinetic parameters to validate that the parameters are not affected by molecular density. In this study, m_r for β_2 integrin–Fc chimera was varied by coupling IgG polyclonal Ab in different concentrations, whereas m_l for ICAM-1 was altered by absorbing the protein in various concentrations, which resulted in two sets of the product $m_r \times m_l$ used in binding kinetics tests. The statistical significance for best-fitted parameters was assessed using the Student t test.

Free and steered molecular dynamics simulation

Crystal structures of LA/HA Mac-1 and LFA-1 I domains as well as ICAM-1 D3 and D1 domains were used (PDB codes of 1JLM (30), 1IDO (31), 1LFA (32), 1T0P (33), and 2OZ4 (34)) to build up the four systems. In this study, LA/HA Mac-1–ICAM-1 D3 and LA/HA LFA-1 I domain–D1 complexes were established by isolating I/D3/D1 domains, docking them together, and replacing Mn^{2+} by Ca^{2+} ion, respectively, as described previously (35). Each complex was solvated into a rectangular water box and the system was then neutralized with ~100 mM Na^+ and Cl^- ions. NAMD program (36) with CHARMM22 all-atom force field (37) was used for molecular dynamics (MD) simulations (i.e., both free MD and steered MD), in which specific parameters were described previously (35, 38). (Simulations were conducted using DeepComp 7000 supercomputer at the Computer Network Information Center, Chinese Academy of Sciences.) In this study, steered MD simulations were conducted to enforce the binding of LA Mac-1 I domain to ICAM-1 D3 domain, because they were unable to be effectively ligated in free MD simulations (35). For this purpose, the metal ion–dependent adhesion site (MIDAS) ion in I domain was fixed and a 200-piconewton force was applied from one of the oxygen atoms of D229 residue side chain in ICAM-1 D3 domain directed to the cation. Then the ligated LA Mac-1–ICAM-1 complex was freely equilibrated for 50 ns to compensate for any inappropriate contacts brought by the force-induced binding procedure and the conformational changes were compared with other three systems. A visual molecular dynamics program was used for data analysis and conformation presentation (39).

Results

Distinct binding affinities of constitutively expressed Mac-1 and LFA-1

We first compared the binding kinetics between Mac-1 and LFA-1 on PMNs. In this study, the expressions of Mac-1 and LFA-1 on isolated PMNs were identified using flow cytometry (left panel in Supplemental Fig. 2A) and then preblocked by incubating the cells, respectively, with anti–LFA-1 and anti–Mac-1 blocking mAbs. Binding of pretreated PMN to ICAM-1–bearing microbead (right panel in Supplemental Fig. 2A) in the presence of Ca^{2+}/Mg^{2+} was measured and the adhesion frequency, P_a, was obtained by subtracting the nonspecific adhesion, P_n (Fig. 1A, dashed lines), from the total adhesion, P_t, using $P_a = (P_t - P_n)/(1 - P_n)$. At a contact duration of t = 0.25~7.0 s, P_a exhibited a transition phase when $t < 2.0$ s and then reached a plateau at a sufficiently long contact duration (Fig. 1A, circle points). These data fitted well with the model predicted using Eq. 1 (Fig. 1A, solid lines). Paired kinetic parameters (A_cK_a, k_r) were estimated from the prediction for each curve and the binding kinetics was compared between Mac-1 and LFA-1 (Fig. 2A–C). It is indicated that the binding affinity, A_cK_a (Fig. 2A), is 11.0-fold enhanced (A_cK_a = [0.09 ± 0.03 and 0.99 ± 0.12] × 10^{-6} μm^4; $p < 0.001$), but the off-rate (Fig. 2B) yields only 1.6-fold increased (k_r = 0.53 ± 0.50 and 0.86 ± 0.31 s^{-1}; p = 0.59) from Mac-1 to LFA-1. This turns out to be a 16.8-fold difference in the on-rate by $A_ck_f = A_cK_a \times k_r$ ([0.05 ± 0.05 and 0.84 ± 0.32] × 10^{-6} μm^{4}s^{-1}; p = 0.03) (Fig. 2C). These results suggest that the enhancement of binding affinity for LFA-1 is mainly attributed to the dramatic increase of on-rate.

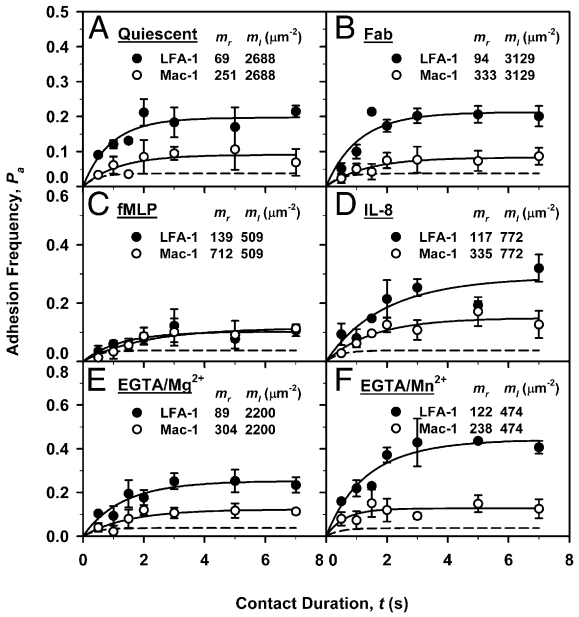

FIGURE 1. Binding curves of constitutively expressed Mac-1 and LFA-1 on PMNs. Mac-1 (○) and LFA-1 (●) on isolated PMNs were preblocked by incubating the cells respectively with anti–LFA-1 (clone MEM-25) and anti–Mac-1 (clone ICRF44) blocking mAbs (**A**, **C**–**F**) or their Fab fragments (**B**). Binding of pretreated PMN to ICAM-1-bearing microbead was measured in the presence of Ca^{2+}/Mg^{2+} (A, B), 10 nM fMLF (C), 10 nM IL-8 (D), 1 mM Mg^{2+} plus 1 mM EGTA (E), or 1 mM Mn^{2+} plus 1 mM EGTA (F) at a duration of t = 0.5~7.0 s, and adhesion frequency, P_a, is presented as the mean ± SEM for more than or equal to three pairs with 100 contacts each duration. Also plotted are the predictions fitted using Eq. 1 (solid lines), whereas the dashed lines represent nonspecific binding of PMNs to blank beads, obtained by fitting Eq. 1 to nonspecific data (not shown for the sake of clarity). m_r and m_l are site densities of β_2 integrin receptors and ICAM-1 ligands, which are determined using a calibration curve obtained from standard beads (Supplemental Fig. 2D).

To exclude the potential impact of integrin cross-linking and PMN activation induced by blocking mAbs (40), we repeated the experiments using Fab fragments, instead of whole IgG mAbs, for Mac-1 or LFA-1 blocking. Again, the adhesion frequency for PMNs pretreated by Fab fragments was quantified, and the data also fitted the model well (Fig. 1B). Although the kinetic parameters estimated (Fig. 2D–F) are slightly reduced compared with whole IgG blocking mAbs (Fig. 2A–C), there are no statistical significance in between. Again, similar difference of kinetic parameters is found from Mac-1 to LFA-1 (i.e., a 11.3-fold enhanced A_cK_a ([0.06 ± 0.02 and 0.68 ± 0.10] × 10^{-6} μm^4; $p <$ 0.001) (Fig. 2D), a 2.5-fold increased k_r [0.30 ± 0.21 and 0.75 ± 0.32 s^{-1}; p = 0.27] (Fig. 2E), and 25.5-fold enhanced A_ck_f ([0.02 ± 0.01 and 0.51 ± 0.23] × 10^{-6} μm^{4}s^{-1}; p = 0.06) (Fig. 2F), respectively). These results suggest that Ab cross-linking may slightly cause integrin activation but not affect the kinetic difference between Mac-1 and LFA-1. Thus, the enhancement of binding affinity for LFA-1 is still mainly attributed to the dramatic increase of on-rate when Fabs of the blocking Abs are used to replace the whole IgG mAbs.

Both Mac-1 and LFA-1 are able to be biochemically or mechanically activated when PMNs are driven to flow over en-

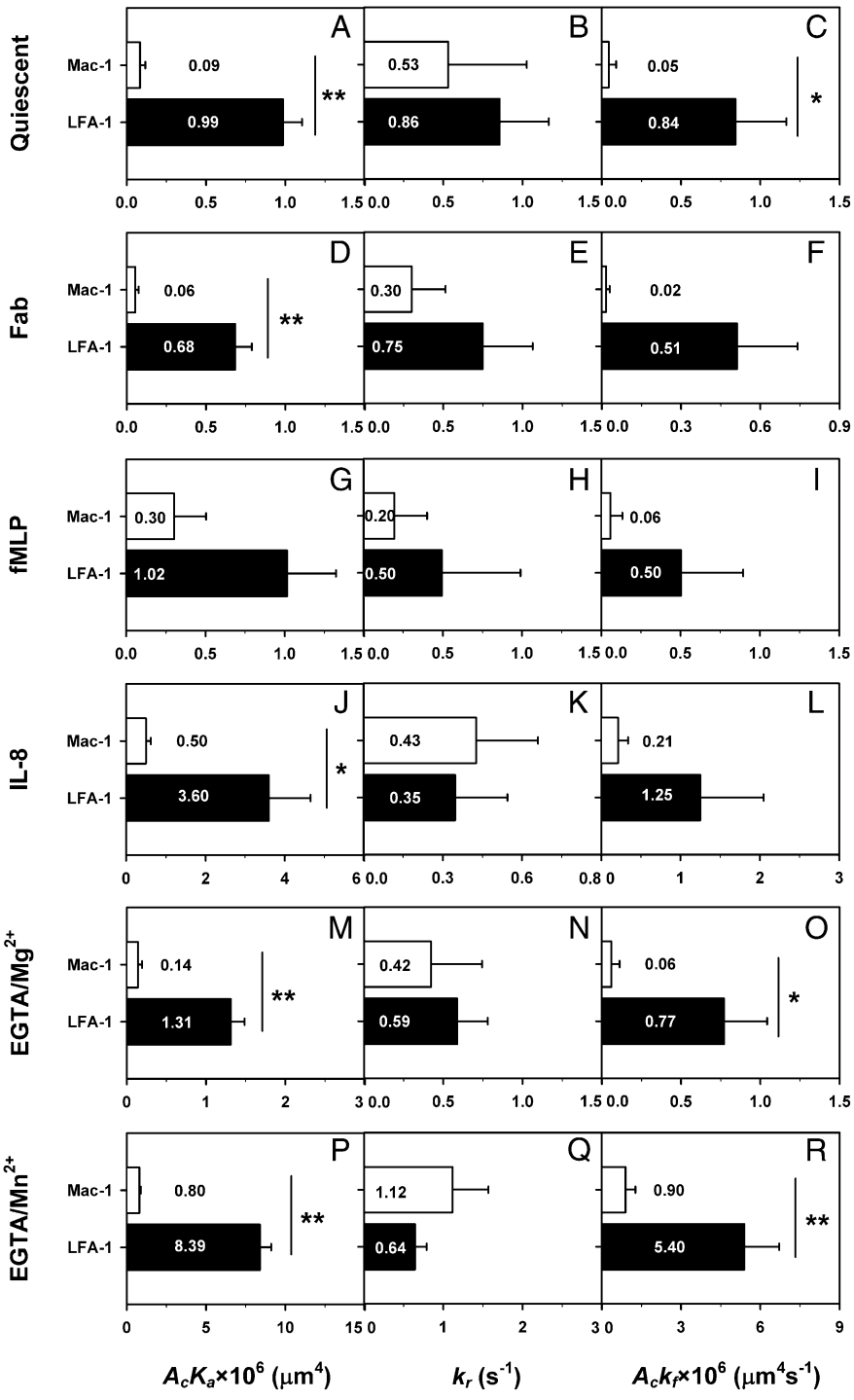

FIGURE 2. Kinetic parameters for constitutively expressed Mac-1 and LFA-1 on PMNs. Kinetic parameters for Mac-1 (□) and LFA-1 (■) on PMNs pretreated, respectively, with anti–LFA-1 and anti–Mac-1 blocking mAbs (**A**–**C**, **G**–**R**) or their Fab fragments (**D**–**F**) were measured in the presence of Ca^{2+}/Mg^{2+} (A–F), 10 nM fMLF (G–I), 10 nM IL-8 (J–L), 1 mM Mg^{2+} plus 1 mM EGTA (M–O), or 1 mM Mn^{2+} plus 1 mM EGTA (P–R). Binding affinity A_cK_a (A, D, G, J, M), off-rate k_r (B, E, H, K, N), and on-rate A_ck_f ($A_cK_a \times k_r$; [C, F, I, L, O]) were obtained by fitting the adhesion frequency P_a versus contact duration t data (Fig. 1A–E) using Eq. 1 after removing the nonspecific adhesion. (P–R) Kinetic parameters were fitted using Eq. 1 from data in Fig. 1F and another independent experiment (data not shown). The best-fit parameters are presented as the means ± SEM, and the values of the kinetic parameters are indicated on the bars separately. The significant differences between Mac-1 and LFA-1 were accessed by Student t test. *$p < 0.05$, **$p < 0.01$.

dothelium (1, 7, 11). To test the impact of PMN activation on β_2-integrn binding kinetics, the cells were stimulated with fMLF (Fig. 1C) or IL-8 (Fig. 1D) to regulate the expression and activation of Mac-1 and/or LFA-1 (21). After fMLF stimulation, the expression of Mac-1 or LFA-1 is ~3-fold (m_r ~712 versus 251 μm^{-2}) or 2-fold (m_r ~139 versus 69 μm^{-2}) increased on activated cells, as compared with those for quiescent cells (inserted values between Fig. 1C and 1A). The binding curves of Mac-1 and LFA-1 are very close to each other (Fig. 1C), which results in 3.3-fold ([0.30 versus 0.09] $\times 10^{-6}$ μm^4) enhanced binding affinity for Mac-1 but similar value ([1.02 versus 0.99] $\times 10^{-6}$ μm^4) for LFA-1 via fMLF stimulation (Fig. 2A, 2G). Moreover, the affinity difference between Mac-1 and LFA-1 is significantly reduced from 11.0-fold (Fig. 2A) to 3.4-fold ([0.30 ± 0.20 and 1.02 ± 0.31] $\times 10^{-6}$ μm^4; $p = 0.08$) (Fig. 2G), resulting from a 2.5-fold (0.20 ± 0.21 and 0.50 ± 0.36 s^{-1}; $p = 0.59$) different k_r (Fig. 2H) and a 8.3-fold ([0.06 ± 0.07 and 0.50 ± 0.40] $\times 10^{-6}$ $\mu m^4 s^{-1}$; $p = 0.29$) distinct A_ck_f (Fig. 2I). By contrast, after IL-8 stimulation, the binding affinity of Mac-1 or LFA-1 is significantly enhanced (5.6- and 3.6-fold for Mac-1 and LFA-1) (Fig. 2J), as compared with those for quiescent cells (Fig. 2A). The affinity is 7.2-fold ([0.50 ± 0.12 and 3.60 ± 1.04] $\times 10^{-6}$ μm^4; $p = 0.01$) higher for LFA-1 than that for Mac-1 (Fig. 2J), corresponding to similar off-rate (0.43 ± 0.23 and 0.35 ± 0.20 s^{-1}; $p = 0.80$) (Fig. 2K) and a 6.0-fold ([0.21 ± 0.13 and 1.25 ± 0.80] $\times 10^{-6}$ $\mu m^4 s^{-1}$; $p = 0.23$) higher on-rate (Fig. 2L). These data indicate that physiologically relevant stim-

ulations via fMLF and IL-8 have great impact on integrin activation in which the major contribution to affinity difference between Mac-1 and LFA-1 also derives from the highly enhanced on-rate, and, moreover, this on-rate difference between Mac-1 and LFA-1 is reduced after integrin activation by fMLF or IL-8. It has been assumed that Mac-1 is the dominant integrin involved in chemotaxis to fMLF, whereas LFA-1 is the major receptor involved in chemotaxis to IL-8 (21), which is not inconsistent with our binding measurements. In fact, fMLF activates PMNs by mainly enhancing Mac-1 avidity, resulting in a similar cellular binding affinity ($A_c m_r m_l K_a$) to that for LFA-1 (Fig. 1C). By contrast, $A_c m_r m_l K_a$ remains lower than that for LFA-1 after IL-8 stimulation (Fig. 1D).

We also tested the effect of Mg^{2+} or Mn^{2+} for Mac-1 and LFA-1 activation (25, 26) (Fig. 1E, 1F). Mg^{2+} stimulation is physiologically relevant but rather weak (41), which only induces slight enhancement of binding affinity (1.6- and 1.3-fold for Mac-1 and LFA-1 from the quiescent state, respectively) (Fig. 2A, 2M). The affinity difference between Mac-1 and LFA-1, however, is still significantly different (i.e., 9.4-fold [0.14 ± 0.05 and 1.31 ± 0.18] × 10^{-6} μm^4; $p < 0.001$) (Fig. 2M), which results from a similar k_r (0.42 ± 0.32 and 0.59 ± 0.19 s^{-1}; $p = 0.67$) (Fig. 2N) but a 12.8-fold enhanced $A_c k_f$ ([0.06 ± 0.05 and 0.77 ± 0.27]×10^{-6} μm^{4}s^{-1}; $p = 0.03$) (Fig. 2O). These results indicate that Mg^{2+} stimulation reserves the on-rate-dominated difference in binding affinity between Mac-1 and LFA-1, even though no remarkable activation is found for each molecule. By contrast, Mn^{2+} stimulation is, even not physiologically relevant, much stronger than Mg^{2+}, as indicated in the high percentage of β_2 integrins recognized by activation reporter mAb MEM-148 binding (Supplemental Fig. 2E) (42) and in the relatively large enhancement of binding affinity (8.9- and 8.5-fold for Mac-1 and LFA-1 from the quiescent state, respectively) (Fig. 2A and 2P). Mn^{2+} stimulation induces a 10.5-fold enhanced $A_c K_a$ from Mac-1 to LFA-1 ([0.80 ± 0.09 and 8.39 ± 0.71] × 10^{-6} μm^4; $p < 0.001$) (Fig. 2P). This affinity difference results from a 0.6-fold reduced k_r (1.12 ± 0.45 and 0.64 ± 0.15 s^{-1}; $p = 0.33$) (Fig. 2Q) and 6.0-fold enhanced $A_c k_f$ ([0.90 ± 0.38 and 5.40 ± 1.32] × 10^{-6} μm^{4}s^{-1}; $p = 0.003$) (Fig. 2R). These data also confirmed the on-rate dominated affinity difference between Mac-1 and LFA-1.

Distinct kinetic features of transfected full-length Mac-1 and LFA-1

Although the blocking protocol has been widely used to isolate the respective impacts of Mac-1 and LFA-1, it is not sure whether the Ab binding could initiate additional outside-in signaling and then affect the binding kinetics of Mac-1 and LFA-1 for quiescent or activated PMNs (40, 43). To determine the impact of the two β_2 integrins independently, we constructed WT full-length Mac-1 and LFA-1 and transfected them into 293T cells. In this study, the target proteins were well expressed (Supplemental Fig. 2B) but absent on mock-transfected cells (data not shown). Binding of the transfected 293T cell to an ICAM-1–coated microbead was measured, and the data (circle points) are consistent with the model (solid lines) (Fig. 3A). In this study, the basal binding affinity of Mac-1 and LFA-1 is 24.2-fold ([2.18 versus 0.09] × 10^{-6} μm^4] and 3.8-fold ([3.79 versus 0.99] × 10^{-6} μm^4) higher, respectively, for 293T cells (Fig. 3C) than those for quiescent PMNs (Fig. 2A). To test this difference, we used MEM-148 mAb, the reporter for the activated swing-out of hybrid domain of β_2 subunit (42), to quantify the activation of Mac-1 and LFA-1. The data confirm that the two integrins (especially Mac-1) are more active in 293T cells with a high percentage of HA conformation than those in PMNs (Supplemental Fig. 2E, 2F). This may be the

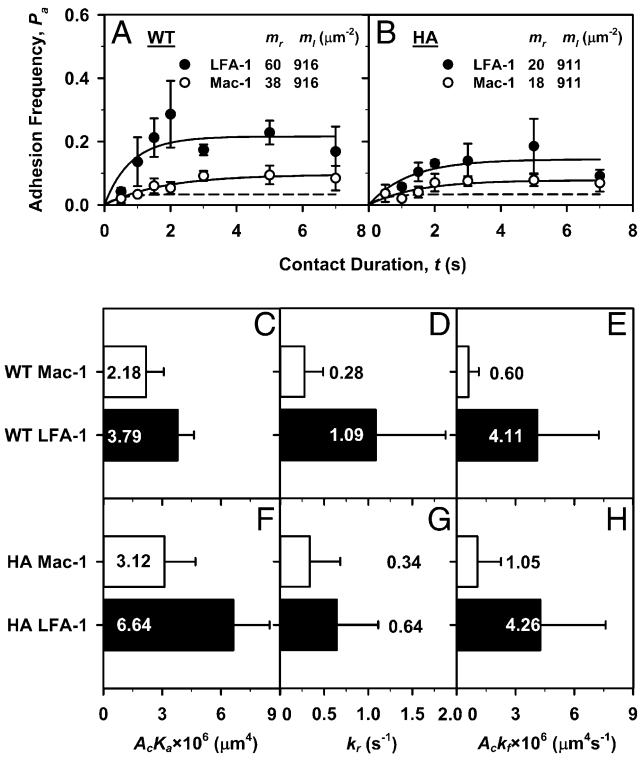

FIGURE 3. Binding kinetics of full-length Mac-1 and LFA-1 transfected on 293T cells. Binding curves (**A**, **B**) and kinetic parameters (**C**–**H**) of full-length WT (A, C–E) and HA (B, F–H) Mac-1 (○) and LFA-1 (●) to ICAM-1 in the presence of Ca^{2+}/Mg^{2+}. (A and B) Adhesion measurements were done at a duration of t = 0.5~7.0 s and adhesion frequency, P_a, is presented as the mean ± SEM for equal to or more than three pairs with 100 contacts each duration. Solid lines denote as the predictions using Eq. 1, whereas the dashed lines represent nonspecific binding of mock transfected 293T to ICAM-1 coated beads. m_r and m_l are site densities of β_2 integrin receptors and ICAM-1 ligands, which are determined using a calibration curve obtained from standard beads (Supplemental Fig. 2D). Binding affinity A_cK_a (C, F), off-rate k_r (D, G), and on-rate A_ck_f ($A_cK_a \times k_r$; [E, H]) were obtained by fitting the data using Eq. 1 after removing the nonspecific adhesion. The best-fit parameters are presented as the means ± SEM, and the values of the kinetic parameters are indicated on the bars separately.

reason why the basal binding affinity of WT Mac-1 and LFA-1 is quite higher in 293T cells and the binding affinity difference of Mac-1 and LFA-1 is significantly reduced to a 1.7-fold ([2.18 ± 0.90 and 3.79 ± 0.84] × 10^{-6} μm^4; $p = 0.22$) (Fig. 3C), as compared with those expressed on quiescent PMNs (11.0-fold different) (Fig. 2A). This results from a 3.9-fold increased k_r (0.28 ± 0.21 and 1.09 ± 0.79 s^{-1}; $p = 0.35$) (Fig. 3D) and a 6.9-fold enhanced $A_c k_f$ ([0.60 ± 0.52 and 4.11 ± 3.14] × 10^{-6} μm^{4}s^{-1}; $p = 0.29$) (Fig. 3E). Nevertheless, these results still demonstrate that the major contribution to affinity difference between Mac-1 and LFA-1 derives from highly enhanced on-rate and moderately increased off-rate.

We also tested the impact of molecular activation of transfected β_2 integrins on their binding kinetics. Because the inside-out signaling induced by chemokines, such as fMLF or IL-8, does not certainly exist in 293T cells, we transfected two mutated Mac-1-Q163C/Q309C and LFA-1-K287C/K294C constructs into 293T cells (Fig. 3B, Supplemental Fig. 2B), which contains, respectively, one disulfate bond to lock the molecule in HA state and the resulted conformations are comparable to those from Mn^{2+} activation (25, 26). Kinetic parameters were then obtained (Fig. 3F–H), and the binding affinity and on-/off-rate are not significantly

enhanced from WT to HA β_2 integrins. The limited increase is presumably due to the basal activation when transfecting WT Mac-1 or LFA-1 into 293T cells (Supplemental Fig. 2F), which confines the further activation when transfecting HA Mac-1 or LFA-1 into 293T cells and then results in the relatively low increase of binding affinity and on-/off-rate between WT and HA states for both Mac-1 and LFA-1 (Fig. 3C–H). In this study, A_cK_a yields a 2.1-fold lower for HA Mac-1 than that for HA LFA-1 ([3.12 ± 1.58 and 6.64 ± 1.85] × 10^{-6} μm^4; $p = 0.18$) (Fig. 3F), which is similar to the difference between two WT β_2 integrins. Again, this results from a 1.9-fold increased k_r (0.34 ± 0.35 and 0.64 ± 0.47 s^{-1}; $p = 0.61$) (Fig. 3G) and a relatively higher 4.0-fold enhanced A_ck_f ([1.05 ± 1.2 and 4.26 ± 3.3] × 10^{-6} $\mu m^4 s^{-1}$; $p = 0.39$) (Fig. 3H). These results support the above observation that similar magnitude enhancement in binding affinity from Mac-1 to LFA-1 is attributed to highly enhanced on-rate and slightly increased off-rate.

On-rate dominated binding of recombinant extracellular Mac-1 and LFA-1

To further isolate the impact of ICAM-1 ligation from that of possible intracellular signaling of full-length β_2 integrins, we constructed WT and HA extracellular Mac-1 and LFA-1 where both α and β subunits of each molecule were fused by Fc fragment (27). ELISA (Supplemental Fig. 3A) and Western blotting (Supplemental Fig. 3B) tests indicated that those proteins were able to bind specifically to their respective mAbs. By presenting respective Mac-1–Fc and LFA-1–Fc onto microbeads via anti-Fc Ab (Supplemental Figs. 2C, 3C), the bindings to ICAM-1 ligands were found to be specific (Supplemental Fig. 3D). Next, we compared the binding kinetics between the two β_2 integrins. Adhesion frequency, P_a, was quantified in the presence of Ca^{2+}/Mg^{2+} at two site densities each. At the given t = 0.25∼7.0 s, the binding curves (points) fitted well with the model (solid lines) (Fig. 4A, 4B). Paired kinetic parameters (A_cK_a, k_r) were estimated from the prediction for each curve, and mean values from the two curves were compared. It is indicated that the affinity is 3.5-fold higher for WT LFA-1–Fc than that for WT Mac-1–Fc (A_cK_a = [0.94 ± 0.24 and 3.29 ± 0.12] × 10^{-6} μm^4; $p = 0.006$) (Fig. 5A), corresponding to a 2.9-fold higher off-rate (k_r = 0.43 ± 0.16 and 1.24 ± 0.11 s^{-1}; p = 0.019) (Fig. 5B) and a 10.5-fold higher on-rate (A_ck_f = [0.39 ± 0.03 and 4.10 ± 0.16] × 10^{-6} $\mu m^4 s^{-1}$; $p = 0.002$) (Fig. 5C). These data also indicate that the major contribution to affinity difference between Mac-1–Fc and LFA-1–Fc derives from highly enhanced on-rate and moderately-increased off-rate.

Although the above activation data for the two β_2-integrins expressed on PMNs and 293T cells were obtained from different ways (i.e., chemokines or divalent cation induced activation and disulfate-bond locked HA state), one may ask about what the potential impacts of such the biochemically induced and structurally based activations on their binding kinetics are. To address this issue, we quantified the impact of activation using same molecular system of β_2 integrin–Fc chimeras. Binding kinetics tests were conducted for HA Mac-1–Fc and LFA-1–Fc constructed by point mutagenesis (Fig. 4C, 4D) and for WT Mac-1–Fc and LFA-1–Fc activated by Mg^{2+} (Fig. 4E, 4F). The reason we did not apply Mn^{2+} to activate WT constructs in this study was that the proteins were found to bind poorly to microbeads in the presence of Mn^{2+} for some unknown reasons. The binding affinity of Mac-1 and LFA-1 increased 2∼3-fold from WT β_2 integrin–Fc chimeras to two activated states (Fig. 5A, 5D, 5G). We also used MEM-148 mAb to quantify the activation of Mac-1–Fc and LFA-1–Fc, which confirmed that the two activation methods were comparable Supplemental Fig. 2G). It has been known that the Mg^{2+} is a weak

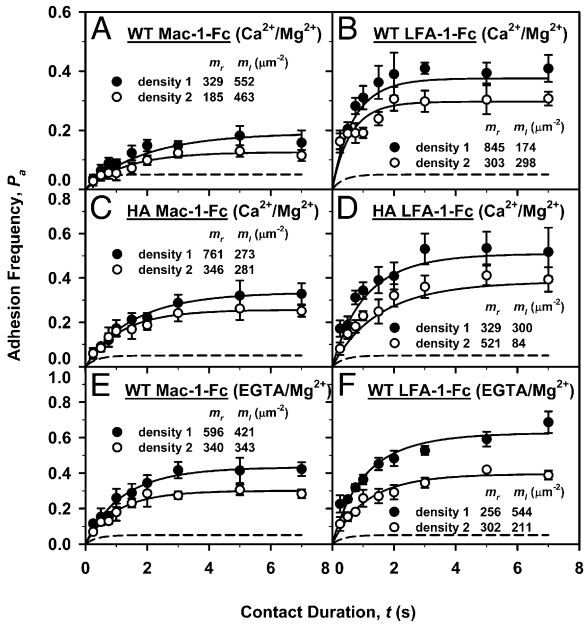

FIGURE 4. Binding curves of recombinant extracellular Mac-1 and LFA-1. Binding curves of extracellular Mac-1–Fc (**A**, **C**, **E**) and LFA-1–Fc (**B**, **D**, **F**) to ICAM-1 in the presence of Ca^{2+}/Mg^{2+} (A–D) or EGTA/Mg^{2+} (E, F). Two sets measurements were done at two different site densities (○, ●) for WT (A, B, E, F) and HA (C, D) at a duration of t = 0.25∼7.0 s, and adhesion frequency, P_a, is presented as the mean ± SEM for at least five pairs with 50 contacts each duration. The solid lines denote as the predictions using Eq. 1. The dashed lines represent nonspecific binding of mock-transfected cell culture to ICAM-1, obtained by fitting nonspecific data (not shown for the sake of clarity) using Eq. 1. m_r and m_l are site densities of β_2 integrin receptors and ICAM-1 ligands, which are determined using a calibration curve obtained from standard beads (Supplemental Fig. 2D).

stimulus inducing intermediate-affinity conformation of integrins (1, 44); therefore, the Mg^{2+} activation is not as effective as Mn^{2+}. The Fc domain of recombinant β_2 integrin may also limit the swing-out of hybrid domain after activation, as seen in the lower percentage of MEM-148 recognition (Supplemental Fig. 2G), which results in that the HA β_2 integrin–Fc protein does not enhance the integrin affinity as effectively as expected comparably to Mn^{2+} (25, 26). Our data presented the similar mechanisms when the same molecules were activated in two different ways. On one hand, a 4.1-fold higher A_cK_a ([2.21 ± 0.57 and 9.13 ± 2.71] × 10^{-6} μm^4; $p = 0.072$) is observed for HA LFA-1–Fc than that for HA Mac-1–Fc, with a similar k_r (0.50 ± 0.11 and 0.63 ± 0.12 s^{-1}; p = 0.376) and a 4.9-fold high A_ck_f ([1.13 ± 0.37 and 5.56 ± 0.43] × 10^{-6} $\mu m^4 s^{-1}$; p = 0.016) (Fig. 5D, 5F). On the other hand, a 3.1-fold higher A_cK_a is found ([2.26 ± 0.31 and 6.93 ± 0.13] × 10^{-6} μm^4; $p = 0.003$) for Mg^{2+}-activated WT LFA-1–Fc than that for WT Mac-1–Fc, corresponding to a similar k_r (0.60 ± 0.09 and 0.55 ± 0.02 s^{-1}; p = 0.9) and a 2.8-fold high A_ck_f ([1.36 ± 0.28 and 3.79 ± 0.14] × 10^{-6} $\mu m^4 s^{-1}$; $p = 0.016$) (Fig. 5G–I). These data indicate that the affinity enhancement from Mac-1 to LFA-1 is comparable in both the biochemically induced and structurally based activations, which is mainly attributed to the enhanced on-rates and the similar off-rates.

Structural differences between Mac-1 and LFA-1 and ICAM-1 interactions

Finally, we tested how such the on-rate–dominated difference in affinity was structurally related. As indicated in the above measurements (summarized in Table I), on-rate is much lower for LA

Table I. Summary of kinetic rates and/or binding affinity of Mac-1 and LFA-1

Integrin[a]	ICAM-1	Assay	Divalent Cation	r_f (pN/s)[b]	A_cK_a (μm^4)	k_r (s^{-1})	A_ck_f ($\mu m^4 s^{-1}$)	Reference
Mac-1–WT (CHO)	sICAM-1	AFM	Ca^{2+}/Mg^{2+}	100–10,000		2.38		(49)
Mac-1–WT (CHO)	sICAM-1	AFM	Mn^{2+}	100–10,000		0.49		(49)
LFA-1–WT (3A9)	sICAM-1	AFM	Ca^{2+}/Mg^{2+}	20–10,000		4		(45)
LFA-1–WT (3A9)	sICAM-1	AFM	Ca^{2+}/Mg^{2+}	10,000–50,000		57		(45)
LFA-1–WT (3A9)	sICAM-1	AFM	Mg^{2+}	20–10,000		0.17		(45)
LFA-1–WT (3A9)	sICAM-1	AFM	Mg^{2+}	10,000–50,000		40		(45)
LFA-1–WT (K562)	sICAM-1	MAT	Ca^{2+}/Mg^{2+}		5.46×10^{-6}	2.01	1.10×10^{-5}	(46)
LFA-1–WT (K562)	sICAM-1	MAT	Mn^{2+}		8.57×10^{-3}	0.19	1.63×10^{-3}	(46)
LFA-1–HA (K562)	sICAM-1	MAT	Ca^{2+}/Mg^{2+}		3.30×10^{-3}	0.42	1.39×10^{-3}	(46)
sLFA-1–WT	sICAM-1	BFP	Mg^{2+}	10–1,000		0.008		(47)
sLFA-1–WT	sICAM-1	BFP	Mn^{2+}	10–1,000		0.02		(47)
sLFA-1–WT	sICAM-1	BFP	Ca^{2+}	10–1,000		2		(47)
LFA-1–WT (PMN)	sICAM-1	BFP	Mg^{2+}	320–8,180		0.1		(41)
LFA-1–WT (PMN)	sICAM-1	BFP	Mg^{2+}/IL-8	46–2,290		0.0002		(41)
LFA-1–WT (PMN)	sICAM-1	BFP	Mg^{2+}/240Q	34–1,800		0.0001		(41)
Mac-1–WT (PMN)	sICAM-1	OT	Ca^{2+}/Mg^{2+}	10	0.09×10^{-6}	0.53	0.05×10^{-6}	Current study
LFA-1–WT (PMN)	sICAM-1	OT	Ca^{2+}/Mg^{2+}	10	0.99×10^{-6}	0.86	0.84×10^{-6}	Current study
Mac-1–WT (PMN)	sICAM-1	OT	fMLF	10	0.30×10^{-6}	0.20	0.06×10^{-6}	Current study
LFA-1–WT (PMN)	sICAM-1	OT	fMLF	10	1.02×10^{-6}	0.50	0.50×10^{-6}	Current study
Mac-1–WT (PMN)	sICAM-1	OT	IL-8	10	0.50×10^{-6}	0.43	0.21×10^{-6}	Current study
LFA-1–WT (PMN)	sICAM-1	OT	IL-8	10	3.60×10^{-6}	0.35	1.25×10^{-6}	Current study
Mac-1–WT (PMN)	sICAM-1	OT	Mg^{2+}	10	0.14×10^{-6}	0.42	0.06×10^{-6}	Current study
LFA-1–WT (PMN)	sICAM-1	OT	Mg^{2+}	10	1.31×10^{-6}	0.59	0.77×10^{-6}	Current study
Mac-1–WT (PMN)	sICAM-1	OT	Mn^{2+}	10	0.80×10^{-6}	1.12	0.90×10^{-6}	Current study
LFA-1–WT (PMN)	sICAM-1	OT	Mn^{2+}	10	8.39×10^{-6}	0.64	5.40×10^{-6}	Current study
Mac-1–WT (293T)	sICAM-1	OT	Ca^{2+}/Mg^{2+}	10	2.18×10^{-6}	0.28	0.60×10^{-6}	Current study
LFA-1–WT (293T)	sICAM-1	OT	Ca^{2+}/Mg^{2+}	10	3.79×10^{-6}	1.09	4.11×10^{-6}	Current study
Mac-1–HA (293T)	sICAM-1	OT	Ca^{2+}/Mg^{2+}	10	3.12×10^{-6}	0.34	1.05×10^{-6}	Current study
LFA-1–HA (293T)	sICAM-1	OT	Ca^{2+}/Mg^{2+}	10	6.64×10^{-6}	0.64	4.26×10^{-6}	Current study
sMac-1–WT	sICAM-1	OT	Ca^{2+}/Mg^{2+}	10	0.94×10^{-6}	0.43	0.39×10^{-6}	Current study
sLFA-1–WT	sICAM-1	OT	Ca^{2+}/Mg^{2+}	10	3.29×10^{-6}	1.24	4.10×10^{-6}	Current study
sMac-1–HA	sICAM-1	OT	Ca^{2+}/Mg^{2+}	10	2.21×10^{-6}	0.50	1.13×10^{-6}	Current study
sLFA-1–HA	sICAM-1	OT	Ca^{2+}/Mg^{2+}	10	9.13×10^{-6}	0.63	5.56×10^{-6}	Current study
sMac-1–WT	sICAM-1	OT	Mg^{2+}	10	2.26×10^{-6}	0.60	1.36×10^{-6}	Current study
sLFA-1–WT	sICAM-1	OT	Mg^{2+}	10	6.93×10^{-6}	0.55	3.79×10^{-6}	Current study

3A9, T cell hybridoma cell line; AFM, atomic force microscopy; BFP, biomembrane force probe; CHO, Chinese hamster ovary cell; K562, human leukemia cell line; MAT, micropipette aspiration technique; OT, optical trap; 240Q, activating mAb to LFA-1; r_f, loading rate used in force spectroscopy measurement; sICAM-1, soluble ICAM-1.

[a]The parentheses in the "Integrin" column denotes the cells used.

Mac-1 than HA Mac-1 as well as LA/HA LFA-1, which means that it is harder for LA Mac-1 to bind ICAM-1. This observation should not be surprised from the structural point of view. In fact, LA Mac-1 I domain is not favorable for ICAM-1 binding but HA Mac-1 and HA/LA LFA-1 I domain is able to bind to ICAM-1 ligand readily in free MD simulations, as reported previously (35). This observation implied that the binding pocket of LA Mac-1 could not open spontaneously, presumably due to the fact that S144 residue prevents the cation in MIDAS from interacting with D229 residue of ICAM-1 D3 domain (Fig. 6A). To further validate this assumption, we conducted a force-induced binding test where the cation in I domain was fixed, and 200 piconewton force was applied by directing one of the oxygen atoms of D229 residue side chain in ICAM-1 D3 domain to the cation. Our simulations indicated that, when the side-chain oxygen atoms OD1 and OD2 of D229 approached the cation (black and red lines), the side-chain oxygen atom OG of S144 moved away (blue line), as exemplified by the distance evolution (Fig. 6B, Supplemental Fig. 4A). It was also indicated that the cation-D229 binding was the most important bond of Mac-1–ICAM-1 interaction (1, 35). After equilibration, the ligated LA Mac-1–ICMA-1 complex presented the interface conformation resembled to that for HA Mac-1–ICMA-1 complex (i.e., with D229 binding to and S144 swinging away from the cation) (Fig. 6C, 6F). Only minor differences appeared in the surrounding water molecules (red spheres) and D140 residue, which bound monodentately to the cation in LA Mac-1 but bidentately to HA Mac-1 ion (Fig. 6C, 6F). Repeated simulations illustrated the similar distance evolution and interface conformation (Supplemental Fig. 4). Thus, these analyses imply that low on-rate for LA Mac-1 measured is presumably due to poor accessibility of the cation to D3 domain, as compared with well-accessible interface for HA Mac-1. For LA/HA LFA-1, S141 and E34 residues of LFA-1 I domain and ICAM-1 D1 domain correspond to S144 and D229 residues of Mac-1 I domain and ICAM-1 D3 domain, respectively. Unlike Mac-1, S141 of HA LFA-1 remains bound to the MIDAS ion without blocking ICAM-1 binding, but S141 of LA LFA-1 runs away (Fig. 6D, 6E). Regardless of the conformation of S141 residue, E34 is able to bind to the cation in LA state and will be strengthened in HA state. This difference between LA and HA LFA-1 binding probably derived from the conformational variation of a chaperone residue, E241 for HA and D239 for LA LFA-1. The former residue was able to hook up the cation with other residues to further present for E34 binding, whereas the latter pushed S141 away and let E34 in (Fig. 6D, 6E). Thus, distinct interface conformations were found between Mac-1 and LFA-1 in different affinity states, which determine the accessibility and availability of MIDAS cation to D3/D1 domain and influence the on-rate value, as measured above experimentally.

We tested the above hypothesis by constructing the site-directed mutation of S144E and S141F for Mac-1–Fc and LFA-1–Fc, respectively. As compared with WT Mac-1-Fc, binding affinity of S144E mutant is 2.1-fold enhanced ($[0.94 \pm 0.17$ and $2.00 \pm 0.89] \times 10^{-6}$ μm^4; $p = 0.24$), mainly because of 1.4-fold higher

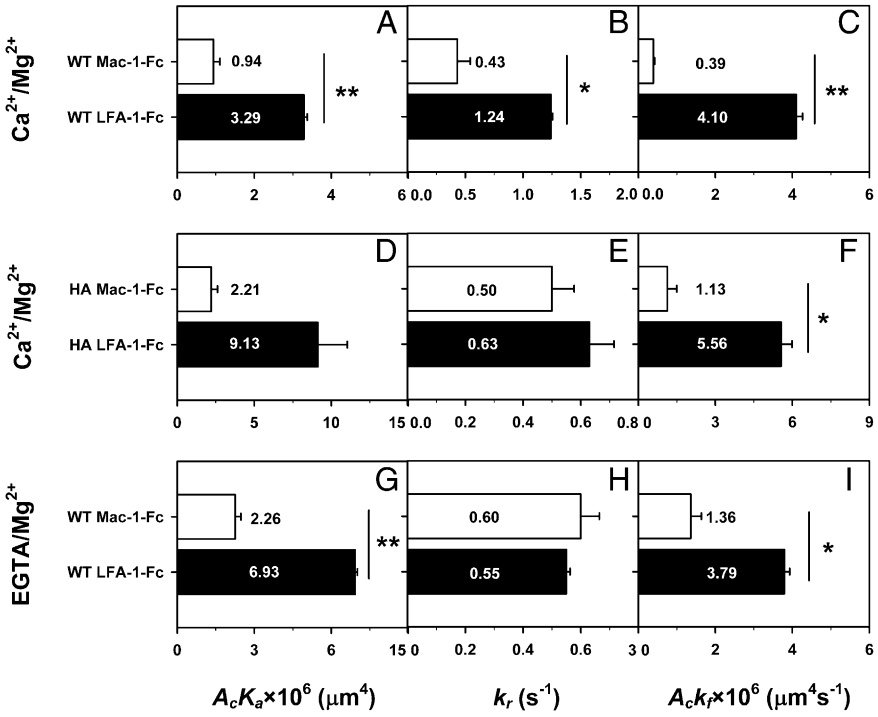

FIGURE 5. Kinetic parameters for recombinant extracellular Mac-1 and LFA-1. Kinetic parameters for extracellular WT Mac-1-Fc (□) and LFA-1-Fc (■) in the presence of Ca^{2+}/Mg^{2+} (**A**–**C**) or EGTA/Mg^{2+} (**G**–**I**). (**D**–**F**) Kinetic parameters for extracellular HA Mac-1–Fc (□) and LFA-1–Fc (■) in the presence of Ca^{2+}/Mg^{2+}. Binding affinity A_cK_a (A, D, G), off-rate k_r (B, E, H), and on-rate A_ck_f ($A_cK_a \times k_r$: [C, F, I]) were obtained by fitting the data using Eq. 1 after removing the nonspecific adhesion and presented as the mean ± SEM from two independent curves. The values of the kinetic parameters are indicated on the bars separately. The significant differences between Mac-1 and LFA-1 were accessed by Student *t* test. $*p < 0.05$, $**p < 0.01$.

on-rate (0.39 ± 0.03 and 0.56 ± 0.55) × 10^{-6} $\mu m^4 s^{-1}$; $p = 0.76$) and 1.5-fold lower off-rate (0.43 ± 0.11 and 0.28 ± 0.22 s^{-1}; $p = 0.59$) (Fig. 7A–C). This variation is mainly due to the prediction that the S-to-E mutation will favor the release and presentation of the MIDAS ion of Mac-1 I domain to the D229 residue of ICAM-1 D3 domain. As compared with WT LFA-1–Fc, binding affinity of S141F mutant is comparable ([3.29 ± 0.09 and 3.82 ± 1.15] × 10^{-6} μm^4; $p = 0.67$) with the 2.9- and 3.4-fold reduced on-rate ([4.10 ± 0.16 and 1.42 ± 0.96] × 10^{-6} $\mu m^4 s^{-1}$; $p = 0.03$) and off-rate (1.24 ± 0.02 and 0.37 ± 0.22 s^{-1}; $p = 0.005$), respectively (Fig. 7D–F). In this study, the S-to-F mutation is designed to expect that the presence of benzene ring of neutralized phenylalanine may block the interactions of MIDAS ion of LFA-1 I domain to the ICAM-1 D1 domain, which reduces the on and off rates simultaneously. These data indicated that the site-directed mutation of even a single residue is able to regulate the binding affinity and kinetic rates, which, at least partially, validates the MD prediction. It is understood that the regulation for single residue mutation on binding kinetics should be limited because other residues with proximity to the binding interface and along

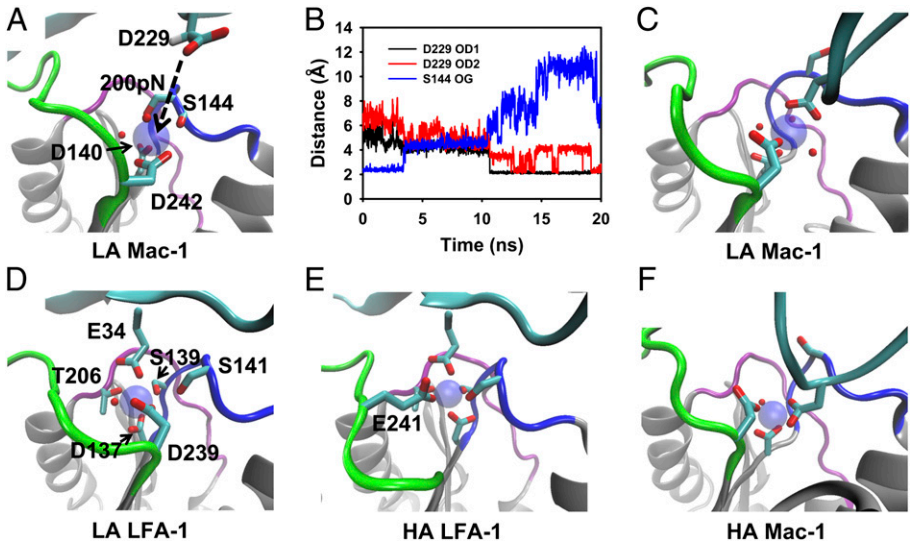

FIGURE 6. Force-induced binding of LA Mac-1 I domain to its ligand ICAM-1 D3 domain and key interactions at the interface between Mac-1/LFA-1 I domain and ICAM-1 D3/D1 domain. (**A**) and (**C**) denote the interface conformations of LA Mac-1–ICAM-1 before and after force-induced binding. (**B**) shows the time course of the distance between the cation in LA Mac-1 and the side-chain oxgens of D229 residue in ICAM-1 D3 or of S144 residue in β_2 integrin I domain. (**D**), (**E**), and (**F**) denote the interface conformations of ICAM-1 to LA LFA-1 (D), HA LFA-1 (E), and HA Mac-1 (F). Three loops of MIDAS (denoted in new cartoon) are respectively colored in blue (β_1-α_1 loop), purple (α_3-α_4 loop), and green (β_4-α_5 loop), and the CD loop located with D229 residue of D3 domain and E34 residue of D1 domain is colored in cyan. Related residues are denoted in licorice and labeled in (A) for Mac-1 (D140, S144, D242) and ICAM-1 D3 (D229) and in (D) and (E) for LFA-1 (D137, S139, S141, T206, D239, E241) and ICAM-1 D1 (E34). Red small spheres are oxygen atoms of water, and blue transparent sphere is the MIDAS ion.

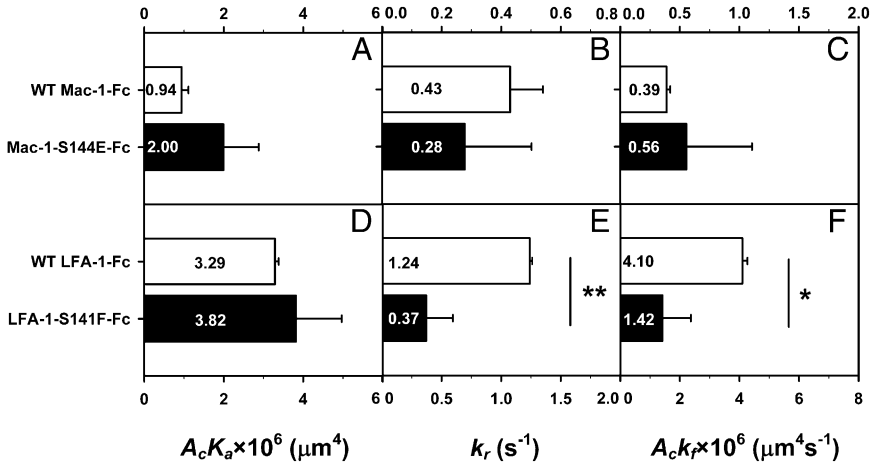

FIGURE 7. Kinetic parameters for site-directed Mac-1–S144E and LFA-1–S141F mutants. (**A**–**C**) Kinetic parameters for extracellular WT (□) and S144E-mutated (■) Mac-1–Fc in the presence of Ca^{2+}/Mg^{2+}. (**D**–**F**) Kinetic parameters for extracellular WT (□) and S141F-mutated (■) LFA-1–Fc in the presence of Ca^{2+}/Mg^{2+}. Binding affinity A_cK_a (A, D), off-rate k_r (B, E), and on-rate A_ck_f ($A_cK_a \times k_r$; [C, F]) were obtained by fitting the data using Eq. 1 after removing the nonspecific adhesion. The best-fit parameters are presented as the means ± SEM. The values of the kinetic parameters are indicated on the bars separately. The significant differences between Mac-1 and LFA-1 were accessed by Student *t* test. $*p < 0.05$, $**p < 0.01$.

the allosteric pathway will also play some roles. It is also noticed that the on-rate dependence of affinity difference is no longer observed, which is not surprised, because identifying a single residue that could ultimately represent the experimental observation of binding affinity is almost impossible.

Discussion

This work attempted to quantify the binding kinetics differences between Mac-1 and LFA-1 and to further the understandings in their distinct functions in inflammatory cascade. Biophysical approaches such as atomic force microscopy (45), micropipette aspiration (46), or biomembrane force probe (41, 47, 48), have been applied in forced dissociation and binding kinetics tests of β_2 integrin and ICAM-1. As summarized in Table I, there are a few works of forced dissociation for Mac-1 or LFA-1 separately (41, 45–47, 49) and one report of binding affinity and kinetic rates for LFA-1 (45). However, much less is known about binding kinetics of Mac-1 to ICAM-1 (49). Here we applied an adhesion frequency approach, a well-known assay for receptor-ligand interactions in cell adhesion (24, 29, 45), to determine the binding kinetics of three β_2-integrin systems (constitutive, transfected full-length or extracellular proteins) in the quiescent or activated states. Similar kinetics difference between Mac-1 and LFA-1 was found in all three systems. Our data indicate that the binding affinity A_cK_a for LFA-1 is much higher than Mac-1 both in the quiescent and activated states, mainly due to the highly-enhanced on-rate A_ck_f and, moreover, this on-rate difference between Mac-1 and LFA-1 is reduced after integrin activation (Figs. 1-5). This may be one of the reasons why LFA-1 could mediate neutrophil slow rolling and firm adhesion in the early stage (12–15) but Mac-1 would play similar or even dominant roles as LFA-1 does after chemokine stimulation (especially with fMLF, Fig. 1C) (3, 16, 17, 21, 23). To the best of our knowledge, this is first time to obtain the binding affinity data for Mac-1 and to compare them with those for LFA-1, which provides an insight to understand their differences in biological functions.

While the on-rate dominated affinity difference of Mac-1 and LFA-1 was found in all three molecular systems, the value of binding affinity varies differently from one to another case. The binding affinity (A_cK_a) presented here is defined to quantify the binding capability per molecule, which is independent of molecular density. We tested this by varying the site density using recombinant integrins (Fig. 4). Two binding curves for each β_2-integrin were obtained at two respective densities of β_2-integrin and ICAM-1. The variance of kinetic parameters fitted using Eq. 1 is trivial from one curve to another (Fig. 5), which implies that the parameters are not affected by molecular density. Thus, the varied expression of β_2-integrin and ICAM-1 from one assay to another is not contributed to the affinity difference among the three molecular systems.

Molecular presentation on the surface is the key factor to determine the binding affinity and on-rate, as we described previously (50, 51). Although all the three types of β_2-integrin molecules yield similar extracellular length with similar orientation, which mostly excludes the impact of molecular length and orientation (51), they are separately presented on the surface with distinct carrier stiffness and microtopology, that is, on cellular membrane and on bead surface. Thus, the difference in binding affinity and on-rate may derive from the difference in their surface presentation, because the carrier stiffness and microtopology of a receptor influences its rate of encountering and binding a surface ligand but does not subsequently affect the stability of binding (51). Various integrin valency stemming from cross-linking or clustering most likely affects the effective site density for binding to its ligand even when same amount of integrins are presented on the surface. Of course, this integrin valency may also be the potential factor to affect the molecular presentation and in turn induces the different binding affinity. Unfortunately, here we are not able to draw any conclusions for integrin valency because it is beyond the scope of the current work. Regardless of this, the affinity difference of Mac-1 and LFA-1 is still on-rate dominated within each assay (Figs. 1–5). Interestingly, this observation is consistent with the previous finding that the affinity difference induced by carrier stiffness and microtopology is mainly on-rate, but not off-rate, dependent (51).

Although the goal of the current work mainly aims at elucidating the binding kinetics and on-rate difference between Mac-1 and LFA-1, we further discussed the off-rate variation of Mac-1 and LFA-1 via various stimuli and compared them with those in the literatures. The off-rate reported previously yields 2.38 and 0.49 s^{-1} for quiescent and activated Mac-1 (49), respectively, and 4∼57 s^{-1} (45) and 0.0001∼40 s^{-1} for quiescent and activated LFA-1 (41, 45–47), respectively, indicating that the off-rates of Mac-1 and LFA-1 are both reduced after activation. In the current work, the off-rate is 0.53 s^{-1} for quiescent Mac-1, and 0.20, 0.43, 0.42, and 1.12 s^{-1} for fMLF, IL-8, Mg^{2+}, and Mn^{2+} stimulation, respectively. Similarly, it yields 0.86 s^{-1} for quiescent LFA-1, 0.50, 0.35, and 0.59 s^{-1} for fMLF, IL-8, and Mg^{2+} activation, as well as 0.64 s^{-1} for Mn^{2+} activation. By excluding the artificial impact of Mn^{2+} activator from the current data set, our results also give out the reduced off-rates of Mac-1 and LFA-1 after activation, which are consistent with those in the literatures.

On-rate dominated affinity difference determined experimentally is well supported by our MD simulations. As indicated in Fig. 6 and Supplemental Fig. 4, the binding pocket remains accessible to the ligand for both LA and HA LFA-1 but switches from close to open conformation when Mac-1 transits from LA to HA state. These simulations implied that Mac-1 binding could be on-rate dominant. The force-induced binding of D3 domain to LA Mac-1 I domain mimics the approaching and squeezing of interacting molecular pair in binding kinetics tests, which enforces Mac-1 I domain to open its pocket for ligand binding. Time duration spent in this extra opening allostery lowers the on-rate value. It is noticed that with limited crystal structures and computational resources, only I domain and D3/D1 domain were employed in the current simulations, which will be extended to the simulations for whole molecule of β_2 integrins. It is also noted that only ICAM-1 ligand was tested in the simulations (and measurements). Future works will involve in multiple ligands which are able to interact with β_2 integrins (especially for Mac-1) and to contribute to firm adhesion and intraluminal crawling (7).

Acknowledgments

We thank Drs. Cheng He (Second Military Medical University, Shanghai, China) and Yan Li (Academy of Military Medical Sciences, Beijing, China) for the cDNA gifts.

Disclosures

The authors have no financial conflicts of interest.

References

1. Luo, B. H., C. V. Carman, and T. A. Springer. 2007. Structural basis of integrin regulation and signaling. *Annu. Rev. Immunol.* 25: 619–647.
2. Hynes, R. O. 2002. Integrins: bidirectional, allosteric signaling machines. *Cell* 110: 673–687.
3. Smith, C. W., S. D. Marlin, R. Rothlein, C. Toman, and D. C. Anderson. 1989. Cooperative interactions of LFA-1 and Mac-1 with intercellular adhesion molecule-1 in facilitating adherence and transendothelial migration of human neutrophils in vitro. *J. Clin. Invest.* 83: 2008–2017.
4. Robinson, M. K., D. Andrew, H. Rosen, D. Brown, S. Ortlepp, P. Stephens, and E. C. Butcher. 1992. Antibody against the Leu-CAM β-chain (CD18) promotes both LFA-1- and CR3-dependent adhesion events. *J. Immunol.* 148: 1080–1085.
5. Meerschaert, J., and M. B. Furie. 1995. The adhesion molecules used by monocytes for migration across endothelium include CD11a/CD18, CD11b/CD18, and VLA-4 on monocytes and ICAM-1, VCAM-1, and other ligands on endothelium. *J. Immunol.* 154: 4099–4112.
6. Slattery, M. J., and C. Dong. 2003. Neutrophils influence melanoma adhesion and migration under flow conditions. *Int. J. Cancer* 106: 713–722.
7. Ley, K., C. Laudanna, M. I. Cybulsky, and S. Nourshargh. 2007. Getting to the site of inflammation: the leukocyte adhesion cascade updated. *Nat. Rev. Immunol.* 7: 678–689.
8. Diamond, M. S., D. E. Staunton, S. D. Marlin, and T. A. Springer. 1991. Binding of the integrin Mac-1 (CD11b/CD18) to the third immunoglobulin-like domain of ICAM-1 (CD54) and its regulation by glycosylation. *Cell* 65: 961–971.
9. Staunton, D. E., M. L. Dustin, H. P. Erickson, and T. A. Springer. 1990. The arrangement of the immunoglobulin-like domains of ICAM-1 and the binding sites for LFA-1 and rhinovirus. *Cell* 61: 243–254.
10. Laudanna, C., and M. Bolomini-Vittori. 2009. Integrin activation in the immune system. *Wiley Interdiscip Rev Syst Biol Med* 1: 116–127.
11. Simon, S. I., M. R. Sarantos, C. E. Green, and U. Y. Schaff. 2009. Leucocyte recruitment under fluid shear: mechanical and molecular regulation within the inflammatory synapse. *Clin. Exp. Pharmacol. Physiol.* 36: 217–224.
12. Dunne, J. L., C. M. Ballantyne, A. L. Beaudet, and K. Ley. 2002. Control of leukocyte rolling velocity in TNF-α-induced inflammation by LFA-1 and Mac-1. *Blood* 99: 336–341.
13. Phillipson, M., B. Heit, P. Colarusso, L. Liu, C. M. Ballantyne, and P. Kubes. 2006. Intraluminal crawling of neutrophils to emigration sites: a molecularly distinct process from adhesion in the recruitment cascade. *J. Exp. Med.* 203: 2569–2575.
14. Kuwano, Y., O. Spelten, H. Zhang, K. Ley, and A. Zarbock. 2010. Rolling on E- or P-selectin induces the extended but not high-affinity conformation of LFA-1 in neutrophils. *Blood* 116: 617–624.
15. Yago, T., B. Shao, J. J. Miner, L. B. Yao, A. G. Klopocki, K. Maeda, K. M. Coggeshall, and R. P. McEver. 2010. E-selectin engages PSGL-1 and CD44 through a common signaling pathway to induce integrin $\alpha_L\beta_2$-mediated slow leukocyte rolling. *Blood* 116: 485–494.
16. Sumagin, R., H. Prizant, E. Lomakina, R. E. Waugh, and I. H. Sarelius. 2010. LFA-1 and Mac-1 define characteristically different intralumenal crawling and emigration patterns for monocytes and neutrophils in situ. *J. Immunol.* 185: 7057–7066.
17. Shulman, Z., V. Shinder, E. Klein, V. Grabovsky, O. Yeger, E. Geron, A. Montresor, M. Bolomini-Vittori, S. W. Feigelson, T. Kirchhausen, et al. 2009. Lymphocyte crawling and transendothelial migration require chemokine triggering of high-affinity LFA-1 integrin. *Immunity* 30: 384–396.
18. Park, E. J., A. Peixoto, Y. Imai, A. Goodarzi, G. Y. Cheng, C. V. Carman, U. H. von Andrian, and M. Shimaoka. 2010. Distinct roles for LFA-1 affinity regulation during T-cell adhesion, diapedesis, and interstitial migration in lymph nodes. *Blood* 115: 1572–1581.
19. Imai, Y., E. J. Park, D. Peer, A. Peixoto, G. Cheng, U. H. von Andrian, C. V. Carman, and M. Shimaoka. 2008. Genetic perturbation of the putative cytoplasmic membrane-proximal salt bridge aberrantly activates α_4 integrins. *Blood* 112: 5007–5015.
20. Semmrich, M., A. Smith, C. Feterowski, S. Beer, B. Engelhardt, D. H. Busch, B. Bartsch, M. Laschinger, N. Hogg, K. Pfeffer, and B. Holzmann. 2005. Importance of integrin LFA-1 deactivation for the generation of immune responses. *J. Exp. Med.* 201: 1987–1998.
21. Heit, B., P. Colarusso, and P. Kubes. 2005. Fundamentally different roles for LFA-1, Mac-1 and α_4-integrin in neutrophil chemotaxis. *J. Cell Sci.* 118: 5205–5220.
22. Lomakina, E. B., and R. E. Waugh. 2010. Signaling and dynamics of activation of LFA-1 and Mac-1 by Immobilized IL-8. *Cell Mol Bioeng* 3: 106–116.
23. Ding, Z. M., J. E. Babensee, S. I. Simon, H. F. Lu, J. L. Perrard, D. C. Bullard, X. Y. Dai, S. K. Bromley, M. L. Dustin, M. L. Entman, et al. 1999. Relative contribution of LFA-1 and Mac-1 to neutrophil adhesion and migration. *J. Immunol.* 163: 5029–5038.
24. Fu, C. L., C. F. Tong, M. L. Wang, Y. X. Gao, Y. Zhang, S. Q. Lü, S. L. Liang, C. Dong, and M. Long. 2011. Determining β2-integrin and intercellular adhesion molecule 1 binding kinetics in tumor cell adhesion to leukocytes and endothelial cells by a gas-driven micropipette assay. *J. Biol. Chem.* 286: 34777–34787.
25. Lu, C., M. Shimaoka, M. Ferzly, C. Oxvig, J. Takagi, and T. A. Springer. 2001. An isolated, surface-expressed I domain of the integrin $\alpha_L\beta_2$ is sufficient for strong adhesive function when locked in the open conformation with a disulfide bond. *Proc. Natl. Acad. Sci. USA* 98: 2387–2392.
26. Shimaoka, M., C. F. Lu, A. Salas, T. Xiao, J. Takagi, and T. A. Springer. 2002. Stabilizing the integrin α_M inserted domain in alternative conformations with a range of engineered disulfide bonds. *Proc. Natl. Acad. Sci. USA* 99: 16737–16741.
27. Coe, A. P. F., J. A. Askari, A. D. Kline, M. K. Robinson, H. Kirby, P. E. Stephens, and M. J. Humphries. 2001. Generation of a minimal $\alpha_5\beta_1$ integrin-Fc fragment. *J. Biol. Chem.* 276: 35854–35866.
28. Zhang, Y., G. Y. Sun, S. Q. Lü, N. Li, and M. Long. 2008. Low spring constant regulates P-selectin-PSGL-1 bond rupture. *Biophys. J.* 95: 5439–5448.
29. Chesla, S. E., P. Selvaraj, and C. Zhu. 1998. Measuring two-dimensional receptor-ligand binding kinetics by micropipette. *Biophys. J.* 75: 1553–1572.
30. Lee, J. O., L. A. Bankston, M. A. Arnaout, and R. C. Liddington. 1995. Two conformations of the integrin A-domain (I-domain): a pathway for activation? *Structure* 3: 1333–1340.
31. Lee, J. O., P. Rieu, M. A. Arnaout, and R. Liddington. 1995. Crystal structure of the A domain from the α subunit of integrin CR3 (CD11b/CD18). *Cell* 80: 631–638.
32. Qu, A., and D. J. Leahy. 1995. Crystal structure of the I-domain from the CD11a/CD18 (LFA-1, $\alpha_L\beta_2$) integrin. *Proc. Natl. Acad. Sci. USA* 92: 10277–10281.
33. Song, G., Y. Yang, J. H. Liu, J. M. Casasnovas, M. Shimaoka, T. A. Springer, and J. H. Wang. 2005. An atomic resolution view of ICAM recognition in a complex between the binding domains of ICAM-3 and integrin $\alpha_L\beta_2$. *Proc. Natl. Acad. Sci. USA* 102: 3366–3371.
34. Chen, X. H., T. D. Kim, C. V. Carman, L. Z. Mi, G. Song, and T. A. Springer. 2007. Structural plasticity in Ig superfamily domain 4 of ICAM-1 mediates cell surface dimerization. *Proc. Natl. Acad. Sci. USA* 104: 15358–15363.
35. Mao, D., S. Lü, N. Li, Y. Zhang, and M. Long. 2011. Conformational stability analyses of α subunit I domain of LFA-1 and Mac-1. *PLoS ONE* 6: e24188.
36. Phillips, J. C., R. Braun, W. Wang, J. Gumbart, E. Tajkhorshid, E. Villa, C. Chipot, R. D. Skeel, L. Kalé, and K. Schulten. 2005. Scalable molecular dynamics with NAMD. *J. Comput. Chem.* 26: 1781–1802.
37. MacKerell, A. D., D. Bashford, M. Bellott, R. L. Dunbrack, J. D. Evanseck, M. J. Field, S. Fischer, J. Gao, H. Guo, S. Ha, et al. 1998. All-atom empirical potential for molecular modeling and dynamics studies of proteins. *J. Phys. Chem. B* 102: 3586–3616.
38. Lü, S., and M. Long. 2005. Forced dissociation of selectin-ligand complexes using steered molecular dynamics simulation. *Mol. Cell. Biomech.* 2: 161–177.
39. Humphrey, W., A. Dalke, and K. Schulten. 1996. VMD: visual molecular dynamics. *J. Mol. Graph.* 14: 33–38, 27–28.
40. Jakus, Z., G. Berton, E. Ligeti, C. A. Lowell, and A. Mócsai. 2004. Responses of neutrophils to anti-integrin antibodies depends on costimulation through low affinity FcγRs: full activation requires both integrin and nonintegrin signals. *J. Immunol.* 173: 2068–2077.
41. Kinoshita, K., A. Leung, S. Simon, and E. Evans. 2010. Long-lived, high-strength states of ICAM-1 bonds to β_2 integrin. II. Lifetimes of LFA-1 bonds under force in leukocyte signaling. *Biophys. J.* 98: 1467–1475.
42. Tang, R. H., E. Tng, S. K. A. Law, and S. M. Tan. 2005. Epitope mapping of monoclonal antibody to integrin $\alpha_L\beta_2$ hybrid domain suggests different requirements of affinity states for intercellular adhesion molecules (ICAM)-1 and ICAM-3 binding. *J. Biol. Chem.* 280: 29208–29216.
43. Lefort, C. T., Y. M. Hyun, J. B. Schultz, F. Y. Law, R. E. Waugh, P. A. Knauf, and M. Kim. 2009. Outside-in signal transmission by conformational changes in integrin Mac-1. *J. Immunol.* 183: 6460–6468.

44. Kong, F., A. J. García, A. P. Mould, M. J. Humphries, and C. Zhu. 2009. Demonstration of catch bonds between an integrin and its ligand. *J. Cell Biol.* 185: 1275–1284.
45. Zhang, X., E. Wojcikiewicz, and V. T. Moy. 2002. Force spectroscopy of the leukocyte function-associated antigen-1/intercellular adhesion molecule-1 interaction. *Biophys. J.* 83: 2270–2279.
46. Zhang, F., W. D. Marcus, N. H. Goyal, P. Selvaraj, T. A. Springer, and C. Zhu. 2005. Two-dimensional kinetics regulation of $\alpha_L\beta_2$-ICAM-1 interaction by conformational changes of the α_L-inserted domain. *J. Biol. Chem.* 280: 42207–42218.
47. Evans, E., K. Kinoshita, S. Simon, and A. Leung. 2010. Long-lived, high-strength states of ICAM-1 bonds to β_2 integrin. I. Lifetimes of bonds to recombinant $\alpha_L\beta_2$ under force. *Biophys. J.* 98: 1458–1466.
48. Chen, W., J. Z. Lou, and C. Zhu. 2010. Forcing switch from short- to intermediate- and long-lived states of the αA domain generates LFA-1/ICAM-1 catch bonds. *J. Biol. Chem.* 285: 35967–35978.
49. Yang, H. Y., J. P. Yu, G. Fu, X. Shi, L. Xiao, Y. Chen, X. Fang, and C. He. 2007. Interaction between single molecules of Mac-1 and ICAM-1 in living cells: an atomic force microscopy study. *Exp. Cell Res.* 313: 3497–3504.
50. Huang, J., J. Chen, S. E. Chesla, T. Yago, P. Mehta, R. P. McEver, C. Zhu, and M. Long. 2004. Quantifying the effects of molecular orientation and length on two-dimensional receptor-ligand binding kinetics. *J. Biol. Chem.* 279: 44915–44923.
51. Wu, L., B. T. Xiao, X. L. Jia, Y. Zhang, S. Q. Lü, J. Chen, and M. Long. 2007. Impact of carrier stiffness and microtopology on two-dimensional kinetics of P-selectin and P-selectin glycoprotein ligand-1 (PSGL-1) interactions. *J. Biol. Chem.* 282: 9846–9854.